journal

J. Am. Ceram. Soc., **95** [9] 2972–2978 (2012)
DOI: 10.1111/j.1551-2916.2012.05301.x

Elastic Properties of Tricalcium Aluminate from High-Pressure Experiments and First-Principles Calculations

Juhyuk Moon,[‡] Seyoon Yoon,[‡] Renata M. Wentzcovitch,[§] Simon M. Clark,[¶,||] and Paulo J.M. Monteiro[‡,†]

[‡]Department of Civil and Environmental Engineering, University of California, Berkeley, California 94720

[§]Department of Chemical Engineering and Materials Science, University of Minnesota, Minneapolis, Minnesota 55455

[¶]Advanced Light Source, Lawrence Berkeley National Laboratory, Berkeley, California 20015

[||]Department of Earth and Planetary Sciences, Macquarie University, North Ryde, North South Wales 2109, Australia

The structure and elasticity of tricalcium aluminate (C_3A) have been experimentally and theoretically studied. From high-pressure X-ray diffraction experiments, the bulk modulus of 102(6) and 110(3) GPa were obtained by fitting second- and third-order finite strain equation of state, respectively. First-principles calculations with a generalized gradient approximation gave an isotropic bulk modulus of 102.1 GPa and an isothermal bulk modulus of 106.0 GPa. The static calculations using the exchange-correlation functional show an excellent agreement with the experimental measurements. Based on the agreement, accurate elastic constants and other elastic moduli were computed. The slight difference of behavior at high pressure can be explained by the infiltration of pressure-transmitting silicone oil into structural holes in C_3A. The computed elastic and mechanical properties will be useful in understanding structural and mechanical properties of cementitious materials, particularly with the increasing interest in the advanced applications at the nanoscale.

I. Introduction

The third most abundant component of ordinary Portland cement is tricalcium aluminate ($Ca_3Al_2O_6$ or C_3A in cement chemistry notation where C = CaO, A = Al_2O_3), which consists of up to 15 wt%. C_3A reacts rapidly with water. Therefore, a relatively small amount has a significant effect upon the early hydration characteristics of a cement paste as well as the long-term sulfate resistance of concrete. Gypsum is added to cement clinker to reduce the rate of reaction of C_3A with water.[1,2] Commercially produced clinkers can contain both cubic and orthorhombic forms of C_3A depending on the availability of alkaline material.[3] In this study, we focus on the cubic phase.

In 1967, Burdick and Day discovered that the cubic form of C_3A contained fourfold coordinated aluminum.[4] Mondal and Jeffery solved the atomic structure using single-crystal X-ray diffraction[5] and found that it has a lattice parameter of 15.263 Å and exists in space group *Pa*3. The unit cell contains 24 $Ca_3Al_2O_3$ units. Ca atoms occupy the 56 body centering positions generated from position ($\frac{1}{8}\frac{1}{8}\frac{1}{8}$) (Fig. 1). The 48 Al atoms and the remaining 16 Ca atoms occupy the corners of the cell. The six AlO_4 tetrahedra in the Al_3O_{18} ring are tilted alternately to each side of the ring. Structural holes (shown in Fig. 1) surrounded by the sixfold rings of AlO_4 tetrahedra facilitate the action of water in hydration process.[5,6]

Calculation of elastic constants is essential because many other parameters related to mechanical properties, such as bulk, shear, and Young's modulus can be derived from them. In addition, C_3A agglomerates may be preserved unhydrated in mature cement pastes, and therefore, affect the global mechanical properties of the cement paste. Velez *et al.* found a value of the Young's modulus as 145 ± 10 GPa using the nanoindentation method and E = 190 ± 10 GPa from resonance frequency technique.[7]

The last few years have seen rapid progress in our understanding of the behavior of the major phases of concrete under pressure from synchrotron high-pressure X-ray diffraction experiments. Compressibility of hydration products of various calcium aluminate hydrates and calcium silicate hydrates has been experimentally investigated.[8–11] On the other hand, application of first-principles calculations has made it possible to theoretically compute the structural and elastic properties of cementitous materials.[12,13] In this study, synchrotron high-pressure X-ray diffraction is used to investigate the crystal structure of the C_3A under pressure. In addition, measurements are supported by first-principles calculations.

The remainder of the present study is organized as follows. In Section II, details of the experimental procedures and results are presented. Section III details the first-principles calculations. The crystalline structure of C_3A is electronically reproduced [Section III(*1*)], then the elastic constants and mechanical properties are calculated [Section III(*2*)]. Section IV compares the experimental results with the computational results.

II. Synchrotron Based High-Pressure X-ray Diffraction

(1) Experimental Procedure

The C_3A was purchased from CTL group (Skokie, IL; http://www.c-t-l.com). Ambient and high-pressure X-ray diffraction measurements were carried out at beamline 12.2.2 of the Advanced Light Source.[14] For the ambient X-ray diffraction measurements, a 350.8130 mm sample-to-detector distance, an X-ray wavelength of 0.6199 Å, and an exposure time of 300 s were used. The sample-to-detector distance, detector tilt angles, and beam position were determined using the NBS LaB_6 powder diffraction standard. The ambient X-ray diffraction pattern is shown in Fig. 2. The measured peak positions and relative intensities of the pattern exactly match those reported by Mondal and Jeffery.[5]

J. Biernacki—contributing editor

Manuscript No. 30977. Received January 18, 2012; approved May 04, 2012.
Supported in part by Award No. KUS-I1-004021, made by King Abdullah University of Science and Technology (KAUST).
†Author to whom correspondence should be addressed. e-mail: monteiro@berkeley.edu

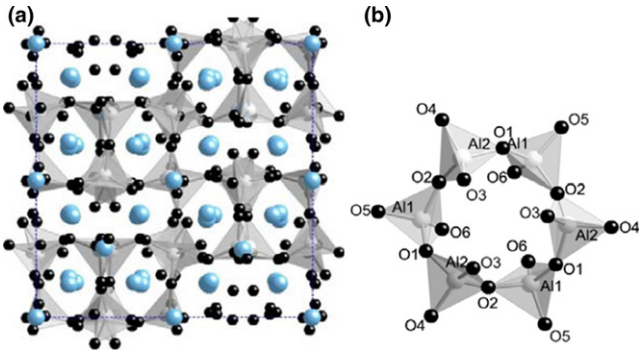

Fig. 1. (a) Optimized crystal structure of tricalcium aluminate (C_3A) and (b) six-member ring of AlO_4 tetrahedra showed along [100] and [-1-1-1] direction, respectively. Gray polyhedra are AlO_4 tetrahedra. Gray, blue, and black spheres represent Al, Ca, and O atoms, respectively.

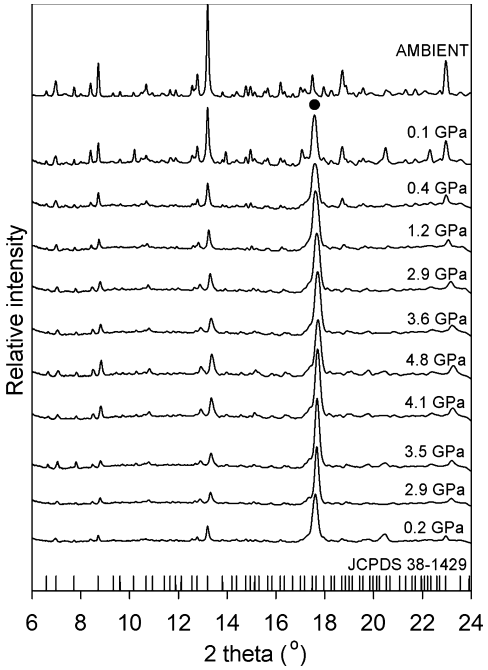

Fig. 2. Integrated powder X-ray diffraction patterns of C_3A as a function of pressure, reported in the 2θ range 6–24° (λ = 0.6199 Å). The below four patterns were collected during decompression. The vertical bottom lines are Bragg peaks positions from Mondal and Jeffery.[5] The filled circle indicates diffraction peaks of ruby.

High pressures were generated using a diamond anvil cell (DAC) fitted with 300 μm culet diamonds. A 125 μm thick piece of stainless steel was use to make the gasket. This was pressed between the diamonds to a thickness of 75 μm and a 180 μm hole was drilled in the center to form the sample chamber. The sample was finely ground and loaded into the gasket hole together silicone oil (a mixture of polysiloxane chains with methyl and phenyl groups), which acted as the pressure-transmitting fluid and a few 2 μm ruby spheres. We waited for 20 min after each pressure increase before collecting data to allow complete equilibration of the sample and pressure-transmitting fluid.

The same sample-to-detector distance (350.8130 mm) and X-ray wavelength (0.6199 Å) as used for the ambient pressure measurement were also used for the high-pressure measurements. An exposure time of 600 s was found sufficient to give an adequate signal to noise ratio. Powder diffraction patterns were collected at intervals between 0.1 and 4.8 GPa with both increasing and decreasing pressure. The pressure was measured using the ruby fluorescence technique.[15] A MAR345 image plate detector (Marresearch GmbH, Norderstedt, Germany) was used to collected X-ray diffraction data. The Fit2D software package[16] was used to convert the diffraction data from 2-D images to conventional plots of intensity versus 2θ. A series of integrated X-ray diffraction patterns at a range of pressures is shown in Fig. 2. The filled circle indicates a strong diffraction peak from the ruby pressure standard.

(2) Experimental Results

The XFit software package[17] was used to determine the positions of the X-ray diffraction peaks in the diffraction patterns shown in Fig. 2 using a series of pseudo-voight peak profiles. Unit-cell parameters and the unit-cell volumes were determined from the peak positions using the Celref software package.[18] At ambient pressure, 25 diffraction peaks were used to refine the unit-cell parameter and volume. Although some of the weak peaks of C_3A disappeared into the background as we increased pressure, 14 peaks remained throughout the pressure range of study, which are enough to calculate an accurate unit-cell parameter and volume. The unit-cell parameters and volumes that we determined are contained in Table I. At ambient pressure with the lattice parameter $a = 15.259(6)$ Å and unit-cell volume $V = 3552$ (1) Å^3 that we determined agree well with a previous study by Mondal and Jeffery, which found $a = 15.263(3)$ Å and $V = 3556(2)$ Å^3.

The ranges of lattice parameters contained in Table I and shown in Fig. 3 are seen to increase at high pressure. This is due to a peak broadening effect in the DAC. A weighted linear least-squares fit was applied to the data to assess both pressure and volume errors.[19] The pressure normalized volume data were fitted by a second- and third- order finite strain equation of state (EoS) (i.e., Murnaghan and Birch-Murnaghan EoS, Fig. 4).[20] As the crystal structure of C_3A is a simple cubic, the finite strain EoS is the ideal EoS for C_3A under hydrostatic pressure. The third-order finite strain EoS is

$$P = \frac{3}{2}K_0\left\{\left(\frac{V}{V_0}\right)^{-\frac{7}{3}} - \left(\frac{V}{V_0}\right)^{-\frac{5}{3}}\right\}\left[1 + \frac{3}{4}(K_0' - 4)\left\{\left(\frac{V}{V_0}\right)^{-\frac{2}{3}} - 1\right\}\right] \quad (1)$$

where V is volume of the unit cell, V_0 is initial volume of the unit cell at ambient pressure, P is the pressure applied to the material, K_0 is the bulk modulus at zero pressure, and K_0' is the derivative of the bulk modulus at zero pressure. By defining the normalized pressure, F and the Eulerian strain, f, the third finite strain EoS is reorganized into the linear form:

$$F(f) = K_0 - 1.5K_0(4 - K_0')f \quad (2)$$

where $F = P/\left\{1.5\left[\left(\frac{V}{V_0}\right)^{-7/3} - \left(\frac{V}{V_0}\right)^{-5/3}\right]\right\}$ and $f = \frac{1}{2}\left[\left(\frac{V}{V_0}\right)^{-2/3} - 1\right]$.

In a plot of F versus f, the y-intercept and slope of graph gives the bulk modulus K_0 and its derivative K_0', which we determined using a weighted linear least-squares fit. The ambient pressure volume, V_0, used in the finite strain EoS was our ambient pressure value of 3552.6 Å.[21] The third-order finite strain EoS when fitted to our experimentally determined volumes gave a goodness of fit parameter $R^2 = 0.998$. We determined a bulk modulus of 110(3) GPa with a derivative of 9.5. In addition, we fitted a second-order finite strain EoS to our data and obtained a bulk modulus of 102(6) GPa.

Table I. Measured Lattice Parameters of Tricalcium Aluminate (C_3A) at Investigated Pressures

Pressure (GPa)	Ambient	0.1(1)	0.4(1)	1.2(2)	2.9(3)	3.6(3)	4.8(4)	4.1(3)	3.5(3)	2.9(3)	0.2(1)
Lattice parameter, a (Å)	15.259 (6)	15.258 (6)	15.256 (6)	15.202 (9)	15.135 (9)	15.11 (2)	15.06 (1)	15.09 (2)	15.12 (2)	15.14 (3)	15.27 (3)
Volume (Å^3)	3552 (1)	3552 (1)	3551 (1)	3513 (2)	3467 (2)	3447 (3)	3415 (2)	3435 (3)	3454 (3)	3468 (5)	3559 (5)

Standard deviations in parentheses.

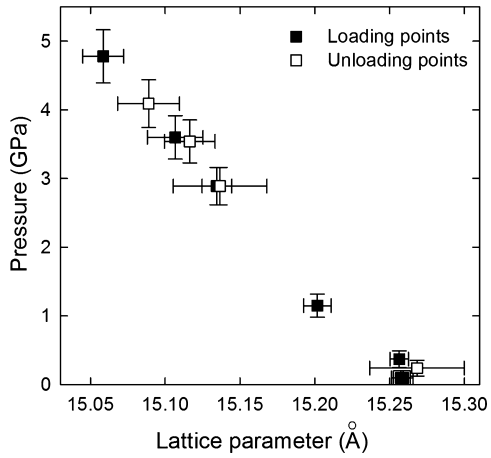

Fig. 3. Structural changes in a unit-cell parameter of C_3A under hydrostatic pressure.

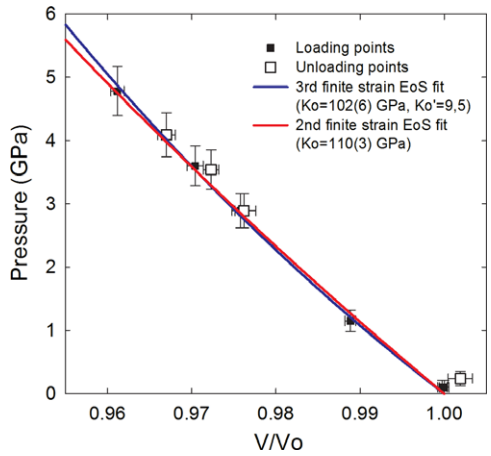

Fig. 4. Normalized unit-cell volume as a function of pressure fitted to the third- and second-order finite strain Equation of State (EoS). Closed and open symbols correspond to experimental data during increasing and decreasing pressure, respectively. Blue and red lines are third- and second-order finite strain EoS fitting curves.

III. First-Principles Calculations

(1) Computational Details

In this section, the theoretical computation is presented. The main problem in quantum mechanics is how to solve the Schrödinger equation for the total wavefunction of a system. Density functional theory (DFT) has been successfully used to solve the equation for a system of interacting electrons in periodic potential sets.[22,23] During the calculation, the exchange-correlation potential is approximated as a functional of electron densities. As the exchange-correlation potential, Perdew–Burke–Ernzerhof (PBE) generalized gradient approximation (GGA)[24] incorporates a dependence on local charge density gradients from a homogeneous electron gas. In addition, the pseudopotential approximation is useful for effective computations. This substitutes the strong potential from the nucleus and core electrons for a slowly varying potential with the same scattering properties.

In this study, all calculations were performed on Linux clusters in the Molecular Graphics and Computation Facility at the University of California, Berkeley. DFT calculations were performed using the PBE-GGA potential for exchange-correlation energy and plane-wave techniques as implemented in the Quantum ESPRESSO distribution.[25] Vanderbilt Ultrasoft pseudopotential,[26] which is highly accurate and allows a low energy cutoff, are generated. The configurations of reference and core radii (r_c) for pseudopotentials have been taken as $3s^2$ $3p^6$ $4s^2$ and r_c = 1.2 Å for Ca, $2s^2$ $2p^6$ $3s^2$ $3p^1$ and r_c = 1.1 Å for Al, and $2s^2$ $2p^4$ and r_c = 0.8 Å for O, respectively.

Table II. Summaries of Atomic Positions of Mondal and Jeffery and Optimized C_3A. Referred to its Symmetry of *Pa*3, the Coordinations of 14 Atoms are Summarized Instead of 264 Atoms

	Mondal and Jeffery 1975[5]			Optimized atomic structure, this study		
	*Pa*3, a = 15.263 Å			*Pa*3, a = 15.39 Å		
	x	y	z	x	y	z
Ca1	0	0	0	0	0	0
Ca2	0.5	0	0	0.5	0	0
Ca3	0.2561 (1)	0.2561 (1)	0.2561 (1)	0.2516	0.2516	0.2516
Ca4	0.3750 (1)	0.3750 (1)	0.3750 (1)	0.3686	0.3688	0.3688
Ca5	0.1386 (1)	0.3763 (1)	0.1272 (1)	0.1421	0.3814	0.1271
Ca6	0.3800 (1)	0.3838 (1)	0.1209 (1)	0.3803	0.3764	0.1204
Al1	0.2526 (1)	0.0133 (1)	0.0197 (1)	0.2517	0.0133	0.0192
Al2	0.2444 (1)	0.2335 (1)	0.0046 (1)	0.2435	0.2298	0.0045
O1	0.2777 (2)	0.1241 (2)	0.0103 (2)	0.2878	0.1227	0.0103
O2	0.4835 (2)	0.1315 (2)	0.2536 (2)	0.4825	0.1300	0.2649
O3	0.2664 (2)	0.2841 (2)	0.1049 (2)	0.2627	0.2823	0.1042
O4	0.2350 (2)	0.4047 (2)	0.2921 (2)	0.2357	0.4027	0.2872
O5	0.3491 (2)	−0.0385 (2)	−0.0174 (2)	0.3467	−0.0463	−0.0098
O6	0.1509 (2)	−0.0104 (2)	−0.0242 (2)	0.1515	−0.0030	−0.0333

Standard deviations in parentheses.

Calculations of elastic properties required precisely relaxed atomic structures and highly converged total energies, forces, and stresses. For special integration points over reciprocal space, a γ-point sampling (i.e., k-points grid of 1 × 1 × 1) of the Brillouin zone was chosen due to the large size of the system (264 atoms in a unit cell). Before calculating structural and elastic properties, a structural optimization was performed to equilibrate the structure at arbitrary pressures. This optimization is important to avoid possible metastable states and to ensure that the relaxed structure is in the region where linear elasticity holds. Both atomic positions and lattice parameters were fully relaxed with strict convergence criteria. For the convergence criteria, a plane-wave cutoff energy of 1000 eV for the wave functions and geometry optimization convergence of 10^{-5} eV for the total energy were used. Although cubic symmetry was not enforced, unit-cell angles remained equal to 90° and lattice parameters remained essentially equal, indicating that a simple cubic symmetry was always found after relaxation. The achieved residual stress components were less than 1 kbar.

The relaxed lattice parameter obtained using this method was found to be 15.39 Å, which is 0.8% larger than that experimentally obtained by us and Mondal and Jeffery.[5] This slight overestimation of the cell parameter is commonly observed when using the PBE-GGA functional form.[27,28] The fractional atomic positions of Mondal and Jeffery and the relaxed cell parameters are summarized in Table II. Due to symmetry equivalence in space group *Pa*3, coordinations of only 14 out of the 264 atoms in the simulation are listed. The results of our calculations show an excellent agreement with the experimental data. The optimized crystal structure and six-member ring of AlO_4 tetrahedra are graphically shown in Fig. 1.

(2) Computational Results

The components of the elastic constant tensor were calculated using standard stress-strain relations.[29,30] The Nielsen-Martin[31] stresses were obtained from the fully relaxed structures. Starting from the relaxed system with lattice parameters $(\vec{a}, \vec{b}, \vec{c}) \equiv (\vec{A})$, the lattice parameters of the strained unit cell $(\vec{a'}, \vec{b'}, \vec{c'}) \equiv (\vec{A'})$ were obtained from the relationship $\vec{A'} = (\vec{I} + \vec{\varepsilon})\vec{A}$, where $\vec{I}$ is the unit matrix and $\vec{\varepsilon}$ is a Lagrangian strain tensor.

Due to the cubic symmetry, C_3A has three independent tensor coefficients: C_{11}, C_{12}, and C_{44}. Two different strains of $\vec{\varepsilon_1}$ and $\vec{\varepsilon_4}$ were applied[30,32]:

$$\vec{\varepsilon}_1 = \begin{pmatrix} \delta & 0 & 0 \\ 0 & 0 & 0 \\ 0 & 0 & 0 \end{pmatrix} \tag{3}$$

$$\vec{\varepsilon}_4 = \begin{pmatrix} 0 & 0 & 0 \\ 0 & 0 & \delta/2 \\ 0 & \delta/2 & 0 \end{pmatrix} \tag{4}$$

where the indices are given in the Voigt notation. Strains of different magnitude (δ = 0.5%, 1%, 1.5%, and 2%) were applied to compute the elastic constants at zero pressure. From the linear relationship between stress σ_i and strain ε_j (Hooke's law),

$$\sigma_i = \sum_{j=1}^{6} C_{ij}\varepsilon_j \tag{5}$$

where C_{ij} are the elastic constants, the linear dependence of the constants on strain could be formulated (Fig. 5). From

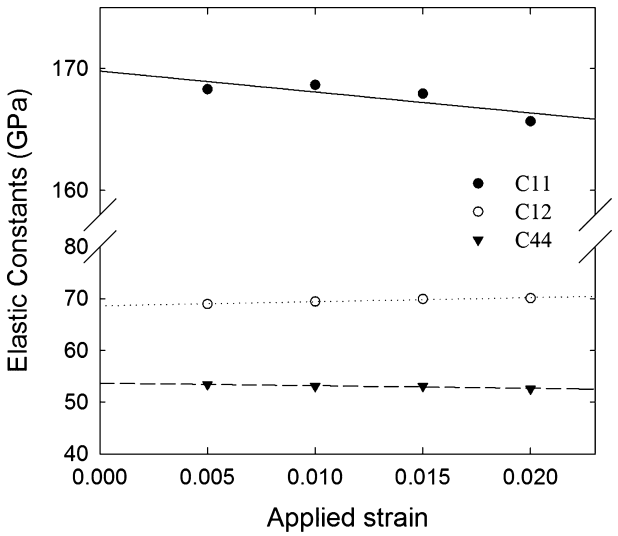

Fig. 5. Computed elastic constants versus applied strains. The solid lines represent linear fits to the calculated values of stress for three elastic stiffness constants.

Table III. Calculated Elastic Constants and Mechanical Properties using Voigt–Reuss–Hill Approximation (VRH)

	This study					Manzano *et al.*[12]
Applied strain	0.5%	1.0%	1.5%	2.0%	At zero pressure	−3% to 3% in steps of 1%
C11 (GPa)	168.3	168.7	167.9	165.7	169.8	172.1
C12 (GPa)	68.9	69.4	69.9	70.1	68.3	68.3
C44 (GPa)	53.4	53.1	53.1	52.6	53.7	56.1
K (GPa)	102.0	102.5	102.6	101.9	102.1	102.9
G (GPa)	51.99 (1)	51.7 (1)	51.4 (1)	50.6 (1)	52.5 (1)	54.4
E (GPa)	133.1	132.7	132.2	130.3	134.4	138.7
η	0.28	0.28	0.29	0.29	0.28	0.28

Standard deviations in parentheses from Voigt–Reuss bound.

the linear fitting of the computed points, the intercepts of the three lines give 169.8, 68.3, and 53.7 GPa for C11, C12, and C44, respectively. The calculated elastic constants are summarized in Table III.

We computed bulk moduli using two different methods. The first method uses the calculated elastic constants for the Voigt–Reuss–Hill (VRH) averages. This method gives a bulk modulus (*K*) and bounds on the shear (*G*) modulus of isotropic poly-crystalline aggregates.[33,34] From the computed *K* and *G*, Young modulus (*E*) and Poisson ratio (η) can be also calculated (Table III). The second method is based on an analysis of the total energies of uniformly compressed states.[20,35] In this case, Eulerian strains are applied and the finite strain EoS is fit to the pressure versus volume relation. Figure 6 shows five computational data points up to 10 GPa and the fitting curve. This gives K_0 = 106.0 GPa, K_0' = 3.8, and V_0 = 3647.4 Å^3. Manzano *et al.* applied first method to compute elastic constants and mechanical properties of C_3A (see Table III). In this study, we applied both methods to compare the results with the high-pressure experiment.

IV. Discussion

High-pressure X-ray diffraction has the unique ability to directly observe the structure of a crystal under pressure, making it possible to obtain the bulk modulus and its pressure derivative. However, because of the extremely small amount of sample in a DAC, the diffraction resolution might not be sufficient to refine the structure, especially for a complex structure at high pressures. In addition, the pressure behavior in the DAC depends on the type of pressure-transmitting medium and various pressure-induced reactions.[10,36] Therefore, it is desirable that high-pressure experimental data should be verified by atomic-level simulations. On the other hand, all atomic-scale computations should be confirmed by experiments. Thus, high-pressure X-ray diffraction technique and first-principle calculations are excellent complementary methods to each other.

Two interesting observations in the experimental results are worth noting. The first is the large K_0' value given by the third finite strain EoS, which indicates that a significant second-order effect in K_0 is not negligible. Figure 4 shows the difference between second- and third-order finite strain EoS fitting at higher pressure. The second observation of note is that the volumes after unloading are slightly expanded compared with those obtained during the loading process. (Fig. 4 and sub plot in Fig. 7). This may be explained by the infiltration of silicone oil into the crystal structure of the C_3A sample. There are 80 cavities in the structure of C_3A (Fig. 1). Seventy-two of these are filled with Ca atoms and the remaining eight cavities are surrounded by sixfold rings of AlO_4 tetrahedra.[5] If molecules of the pressure-transmitting medium are small enough to enter the cavities then the volume compressibility would become lower than that measured with a non-penetrating fluid.[10,11] Therefore, as the structural cavities fill with silicone oil, the structure becomes stiffer,

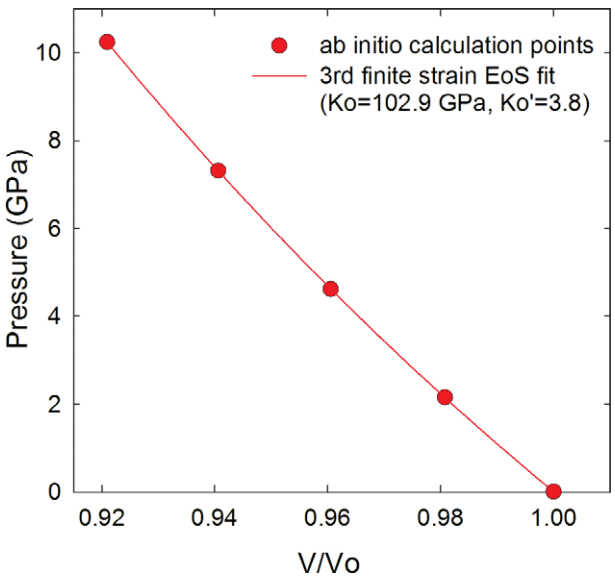

Fig. 6. Calculated structural changes under pressure. The circles represent our ab initio computation results. The red line corresponds to third-order finite strain Equation of State fitting, which yields K_0 = 106.0 GPa and K_0' = 3.8.

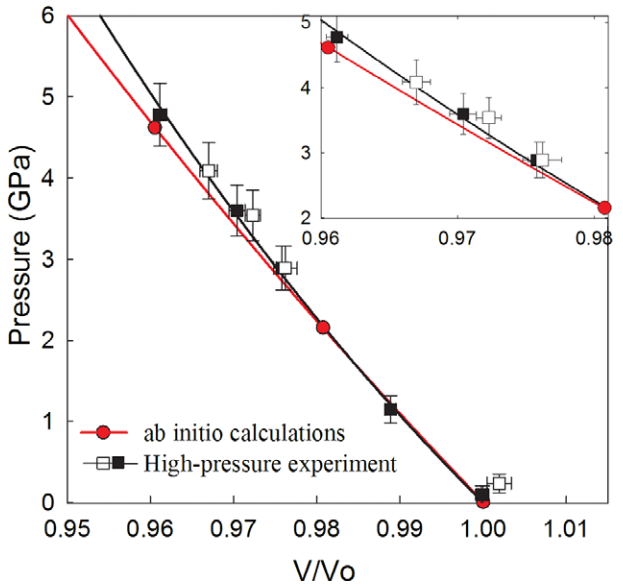

Fig. 7. Experimental and computational normalized volumes versus pressures. Closed and open symbols represent the experimental data during increasing and decreasing pressure, respectively. The red circles represent ab initio computation data points. The black and red lines correspond to third finite strain EoS curves fitted to the experimental and computational data, respectively. Due to the smaller pressure derivative in computation, there is a slight difference over 3 GPa.

Table IV. Comparison of the Results of the High-Pressure Experiments and *Ab Initio* Calculations. To Compute the Bulk Modulus and its Derivative, Second- and Third-order Finite Strain Equation of State (EoS) were Used

		Lattice parameter, a (Å)	Volume (Å^3)	K_0'	K_0 (GPa)
High pressure experiment (this study)	Third finite strain EoS	15.254(6)	3549(1)	9.5	102(6)
	Second finite strain EoS	15.254(6)	3549(1)	4	110(3)
Ab initio calculations (this study)	VRH approximation	15.39	3645.2	n.d	102.1
	Third finite strain EoS	15.39	3647.4	3.8	106.0
Ab initio calculations (Manzano *et al.*[12])	VRH approximation	15.38	3638.1	n.d	102.9

n.d: not determined

which gives a larger K_0'. The infiltration of silicone oil can also explain the unexpected volume expansion during unloading.

It was not possible to include this effect in our simulations. In theoretical calculations, the stiffness of the atomistic framework itself is of concern. First, the atomic structure of C_3A was reproduced by full relaxation of the structural parameters using damped variable cell shape molecular dynamics.[25] This allows lattice parameters and atomic positions to move until both the energy and force convergence criteria are satisfied. Then, elastic constants were computed. This stress-strain approach determined elastic constants for which isothermal and adiabatic values are identical by calculating forces for strained configurations. Next, the VRH approximation was applied to compute the average bulk modulus of an isotropic poly-crystalline aggregate. Consistent results were obtained for the relaxed structure and elastic constants determined by Manzano *et al.* (Table III) within the 3% error range.

In our experiment, the isothermal bulk modulus was determined from the EoS parameters. Calculations were performed to simulate isotropic experimental conditions and direct comparison between experimental and computational pressure versus volume is possible as summarized in Table IV and Fig. 7. A slightly larger value of K_0, 106 GPa, is obtained by fitting the finite strain EoS, than the VRH average of K_0, 102 GPa. This difference is expected, as VRH averages correspond to the averaged bulk modulus of polycrystalline aggregates. However, the level of agreement of isothermal bulk modulus between theory and experiments is precisely what is expected from GGA-PBE calculations: larger equilibrium volumes and smaller bulk modulus when compared with experiments.[27,28]

The overall pressure behavior and isothermal bulk modulus are in excellent agreement with the DFT calculation. As the experimental isothermal bulk modulus agreed well with the theoretical bulk modulus, the computed elastic tensor coefficients for C_3A are also reliable. These elastic coefficients and the isothermal bulk modulus are fundamental material properties and knowing them will allow us to better understand the characteristics of clinker materials. In Portland cement clinker, various cations can be substituted in the large interstitial cavities in C_3A. The experimental and computational consistence reported here gives great credibility to the computational approach to understanding the effects of impurities on clinker materials.[37]

Acknowledgments

The Advanced Light Source is supported by the Director, Office of Science, Office of Basic Energy Sciences, of the U.S. Department of Energy under Contract No. DE-AC02-05CH11231. RMW was supported by NSF/EAR 1047629. The UC Berkeley Molecular Graphics and Computation Facility is supported by NSF/CHE-0840505.

References

[1]P. K. Mehta and P. J. M. Monteiro, *Concrete: Microstructure, Properties and Materials*, 3rd edition. eMcGraw-Hill Companies, New York, NY, 2006.

[2]H. F. W. Taylor, *Cement Chemistry*, 2nd edition. Thomas Telford, London, 1997.

[3]I. Maki, "Nature of the Prismatic Dark Interstitial Material in Portland Cement Clinker," *Cem. Concr. Res.*, **3** [3] 295–313 (1973).

[4]V. L. Burdick and D. E. Day, "Coordination of Aluminum Ions in Tricalcium Aluminate," *J. Am. Ceram. Soc.*, **50** [2] 97–101 (1967).

[5]P. Mondal and W. Jeffery, "The Crystal Structure of Tricalcium Aluminate, $Ca_3Al_2O_6$," *Acta Crystallogr.*, **31**, 689–97 (1975).

[6]M. Collepardi, G. Baldini, and M. Pauri, "Tricalcium Aluminate Hydration in the Presence of Lime, Gypsum or Sodium sulfate," *Cem. Concr. Res.*, **8** [5] 571–80 (1978).

[7]K. Velez, S. Maximilien, D. Damidot, G. Fantozzi, and F. Sorrentino, "Determination by Nanoindentation of Elastic Modulus and Hardness of Pure Constituents of Portland Cement Clinker," *Cem. Concr. Res.*, **31** [4] 555–61 (2001).

[8]S. M. Clark, B. Colas, M. Kunz, S. Speziale, and P. J. M. Monteiro, "Effect of Pressure on the Crystal Structure of Ettringite," *Cem. Concr. Res.*, **38** [1] 19–26 (2008).

[9]J. Oh, S. M. Clark, and P. J. M. Monteiro, "Does the Al substitution in C-S-H(I) change its mechanical property?" *Cem. Concr. Res.*, **41** [1] 102–6 (2011).

[10]J. Moon, J. Oh, M. Balonis, F. P. Glasser, S. M. Clark, and P. J. M. Monteiro, "Pressure Induced Reactions Amongst Calcium Aluminate Hydrate Phases," *Cem. Concr. Res.*, **41** [6] 571–8 (2011).

[11]J. Moon, J. Oh, M. Balonis, F. P. Glasser, S. M. Clark, and P. J. M. Monteiro, "High Pressure Study of Low Compressibility Tetracalcium Aluminum Carbonate Hydrates $3CaO{\cdot}Al_2O_3{\cdot}CaCO_3{\cdot}11H_2O$," *Cem. Concr. Res.*, **42** [1] 105–10 (2012).

[12]H. Manzano, J. S. Dolado, and A. Ayuela, "Structural, Mechanical, and Reactivity Properties of Tricalcium Aluminate using First-Principles Calculations," *J. Am. Ceram. Soc.*, **92** [4] 897–902 (2009).

[13]R. Shahsavari, R. J. M. Pellenq, and F. Ulm, "First-Principles Study of Elastic Constants and Interlayer Interactions of Complex Hydrated Oxides: Case Study of Tobermorite and Jennite," *J. Am. Ceram. Soc.*, **92** [10] 2323–30 (2009).

[14]M. Kunz, A. A. MacDowell, W. A. Caldwell, D. Cambie, R. S. Celestre, E. E. Domning, R. M. Duarte, A. E. Gleason, J. M. Glossinger, N. Kelez, D. W. Plate, T. Yu, J. M. Zaug, H. A. Padmore, R. Jeanloz, A. P. Alivisatos, and S. M. Clark, "A beamline for High-Pressure Studies at the Advanced Light Source with a Superconducting Bending Magnet as the Source," *J. Synchrotron Radiat.*, **12** [5] 650–8 (2005).

[15]H. K. Mao, J. Xu, and P. M. Bell, "Calibration of the Ruby Pressure Gauge to 800 kbar Under Quasi-Hydrostatic Conditions," *J. Geophys. Res.*, **91** [5] 4673–6 (1986).

[16]A. P. Hammersley, S. O. Svensson, M. Hanfland, A. N. Fitch, and D. Hcousermann, "Two-Dimensional Detector Software: From Real Detector to Idealised Image or Two-Theta Scan," *High Pressure Res.*, **14**, 235–48 (1996).

[17]R. W. Cheary and A. A. Coelho, *Programs XFIT and FOURYA, deposited in CCP14 Powder Diffraction Library*. Engineering and Physical Sciences Research Council, Daresbury Laboratory, Warrington, England, 1996.

[18]J. Laugier and B. Bochu, *CELREF. Version 3. Cell Parameter Refinement Program from Powder Diffraction Diagram*. Laboratoire des Matériaux et du Génie Physique, Ecole Nationale Supérieure de Physique de Grenoble (INPG), France, 2002.

[19]B. C. Reed, "Linear Least-Squares Fits with Errors in Both Coordinates," *Am. J. Phys.*, **57** [7] 642–6 (1989).

[20]F. Birch, "Finite Strain Isotherm and Velocities for Single-Crystal and Polycrystalline NaCl at High Pressures and 300 K," *J. Geophys. Res.*, **83** [B3] 1257–68 (1978).

[21]R. Jeanloz, "Finite-Strain Equation of State for High-Pressure Phases," *Geophys. Res. Lett.*, **8** [12] 1219–22 (1981).

[22]P. Hohenberg and W. Kohn, "Inhomogeneous Electron Gas," *Phys. Rev.*, **136** [3B] B864–71 (1964).

[23]W. Kohn and L. J. Sham, "Self-Consistent Equations Including Exchange and Correlation Effects," *Phys. Rev.*, **140** [4A] A1133–8 (1965).

[24]J. P. Perdew, K. Burke, and M. Ernzerhof, "Generalized Gradient Approximation Made Simple," *Phys. Rev. Lett.*, **77** [18] 386–8 (1996).

[25]P. Giannozzi, S. Baroni, N. Bonini, M. Calandra, R. Car, C. Cavazzoni, D. Ceresoli, G. L. Chiarotti, M. Cococcioni, I. Dabo, A. D. Corso, S. de Gironcoli, S. Fabris, G. Fratesi, R. Gebauer, U. Gerstmann, C. Gougoussis, A. Kokalj, M. Lazzeri, L. Martin-Samos, N. Marzari, F. Mauri, R. Mazzarello, S. Paolini, A. Pasquarello, L. Paulatto, C. Sbraccia, S. Scandolo, G. Sclauzero, A. P. Seitsonen, A. Smogunov, P. Umari, and R.M. Wentzcovitch, "QUANTUM ESPRESSO: A Modular and Open-Source Software Project for Quantum Simulations of Materials," *J. Phys. Condens. Matter*, **21** [39] 395502, 19pp (2009).

[26]D. Vanderbilt, "Soft Self-Consistent Pseudopotentials in a Generalized Eigenvalue Formalism," *Phys. Rev. B*, **41** [11] 7892–5 (1990).
[27]H. Yao, L. Ouyang, and W. Y. Ching, "Ab Initio Calculation of Elastic Constants of Ceramic Crystals," *J. Am. Ceram. Soc.*, **90** [10] 3194–204 (2007).
[28]Th. Demuth, Y. Jeanvoine, J. Hafner, and J. G. Angyan, "Polymorphism in Silica Studied in the Local Density and Generalized-Gradient Approximations," *J. Phys. Condens. Matter*, **11** [19] 3833–74 (1999).
[29]R. M. Wentzcovitch, N. L. Ross, and G. D. Price, "Ab Initio Study of $MgSiO_3$ and $CaSiO_3$ Perovskites at Lower Mantle Pressures," *Phys. Earth Planet. Int.*, **90** [101] 101–12 (1995).
[30]B. B. Karki, L. Stixrude, and R. M. Wentzcovitch, "High-Pressure Elastic Properties of Major Materials of Earth's Mantle From First Principles," *Rev. Geophys.*, **39** [4] 507–34 (2001).
[31]O. H. Nielsen and R. M. Martin, "First-Principles Calculation of Stress," *Phys. Rev. Lett.*, **50** [9] 697–700 (1983).
[32]B. B. Karki, G. J. Ackland, and J. Crain, "Elastic Instabilities in Crystals from Ab Initio Stress-Strain Relations," *J. Phys. Condens. Matter*, **9** [41] 8579–89 (1997).
[33]R. Hill, "The Elastic Behaviour of a Crystalline Aggregate," *Proc. Phys. Soc. Sect. A*, **65** [5] 349–54 (1952).
[34]J. P. Watt, G. F. Davies, R. J. O'Connell, and R. J, "The Elastic Properties of Composite Materials," *Rev. Geophys.*, **14** 541–63 (1976).
[35]J. P. Poirier, *Introduction of the Physics of Earth Interior*, Vol. 83, 2nd edition. Cambridge University Press, Cambridge, UK, 2000.
[36]M. Colligan, P. M. Forster, A. K. Cheetham, Y. Lee, T. Vogt, and J. A. Hriljac, "Synchrotron X-ray Powder Diffraction and Computational Investigation of Purely Siliceous Zeolite Y under Pressure," *J. Am. Chem. Soc.*, **126** [38] 12015–22 (2004).
[37]H. Manzano, E. Durgun, M. J. A. Qomi, F. J. Ulm, R. J. M. Pellenq, and J. C. Grossman, "Impact of Chemical Impurities on the Crystalline Cement Clinker Phases Degermined by Atomistic Simulation.," *Cryst. Growth Des.*, **11** [7] 2964–72 (2011). □